GLIA 56:1463–1477 (2008)

Morphogenesis and Regulation of Bergmann Glial Processes During Purkinje Cell Dendritic Spine Ensheathment and Synaptogenesis

JOCELYN J. LIPPMAN,[1] TAMAR LORDKIPANIDZE,[1] MARGARET E. BUELL,[1] SUNG OK YOON,[2] AND ANNA DUNAEVSKY[1]*

[1]*Department of Neuroscience, Brown University, Box G-LN, Providence, Rhode Island*
[2]*Center for Molecular Neurobiology, Department of Molecular and Cellular Biochemistry, Ohio State University, Columbus, Ohio*

KEY WORDS
Bergmann glia; dendritic spines; synaptogenesis; Purkinje cell; cerebellum; Rac1

ABSTRACT
Astrocytes have an important role in synaptic formation and function but how astrocytic processes become associated with synaptic structures during development is not well understood. Here we analyzed the pattern of growth of the processes extending off the main Bergmann glial (BG) shafts during synaptogenesis in the cerebellum. We found that during this period, BG process outgrowth was correlated with increased ensheathment of dendritic spines. In addition, two-photon time-lapse imaging revealed that BG processes were highly dynamic, and processes became more stable as the period of spine ensheathment progressed. While process motility was dependent on actin polymerization, activity of cytoskeletal regulators Rac1 and RhoG did not play a role in glial process dynamics or density, but was critical for maintaining process length. We extended this finding to probe the relationship between process morphology and ensheathment, finding that shortened processes result in decreased coverage of the spine. Furthermore, we found that areas in which BG expressed dn-Rac1, and therefore had a lower level of synaptic ensheathment, showed an overall increase in synapse number. These analyses reveal how BG processes grow to surround synaptic structures, elucidate the importance of BG process structure for proper development of synaptic ensheathment, and reveal a role for ensheathment in synapse formation.

INTRODUCTION

Although glia are more numerous than neurons, their vital roles in complex brain functioning are poorly understood. Studies spanning the last decade revealed new aspects of the neuron/glial relationship beyond maintenance of the milieu, especially in synaptic function, plasticity, and spine and dendrite development (Amateau and McCarthy, 2002; Araque et al., 1998; Christopherson et al., 2005; Ge et al., 2006; Laming et al., 2000; Lin and Bergles, 2004; Lordkipanidze and Dunaevsky, 2005; Murai et al., 2003; Pfrieger and Barres, 1997; Takatsuru et al., 2006; Takayasu et al., 2006; Ullian et al., 2001; Yang et al., 2003; Zhang et al., 2003). The intimate morphological relationship between glial processes and synapses provides an opportunity for such interactions (Halassa et al., 2007). The importance of glial ensheathment in synaptic function is underscored by impairment of memory tasks and altered synaptic plasticity in mice with altered glial protein expression (Gerlai et al., 1995; McCall et al., 1996; Shibuki et al., 1996). Synapse ensheathment by glia occurs throughout the brain, but the degree of coverage varies by region (Grosche et al., 1999; Peters et al., 1976; Spacek, 1985; Ventura and Harris, 1999). In the cerebellum, almost every synapse onto a Purkinje cell (PC) is ensheathed by Bergmann glia (BG) (Grosche et al., 1999; Spacek, 1985).

Early in development, BG extend smooth radial processes to the pial surface from their somas in the Purkinje layer. BG shafts provide scaffolding for granule cell migration (Altman, 1972; Gregory et al., 1988; Hatten and Mason, 1990; Rakic, 1971) and direct growth of PC dendrites (Lordkipanidze and Dunaevsky, 2005; Yamada et al., 2000). After the bulk of granule cell migration is complete, lateral processes emerge from BG shafts, coincident with the expansion of the PC dendritic tree and synaptogenesis. The temporal correlation between glial process development and synaptogenesis suggests a role for ensheathment in synaptic development and maturation (Grosche et al., 1999; Yamada et al., 2000). Yet, the morphogenesis and regulation of glial sheath development, and their role during synaptic formation, have not been previously studied.

In this study, we investigate morphological and dynamic properties of BG processes in the developing cerebellum, how they grow to ensheath synapses, and the involvement of ensheathment in synapse formation. We examine two ages relevant to synapse formation and dendritic spine motility: at postnatal day (P)10 dendritic spines are highly motile and synaptogenesis peaks,

Additional Supporting Information may be found in the online version of this article.

Grant sponsor: NINDS; Grant number: 1R01NS057667; Grant sponsor: Whitehall Foundation.

*Correspondence to: Anna Dunaevsky, Assistant Professor, Department of Neuroscience, Brown University, 185 Meeting St., Providence, RI 02912, USA. E-mail: Anna_Dunaevsky@brown.edu

Received 10 August 2007; Revised 25 April 2008; Accepted 30 April 2008

DOI 10.1002/glia.20712

Published online 9 July 2008 in Wiley InterScience (www.interscience.wiley.com).

while at P20 synaptogenesis reaches a plateau and spine motility decreases (Dunaevsky et al., 1999). Using 2-photon imaging of BG fluorescently labeled via *in vivo* viral injections or biolistics in slice culture, we find that glial processes are highly dynamic and their motility is developmentally regulated. Glial processes also dramatically increase in number and complexity between these periods. Our confocal and electron microscopy analysis demonstrates that the developmental increase in glial process complexity correlates with increased ensheathment of synapses. Perturbation of glial process length also leads to reduced ensheathment of synapses. Finally, decreasing the level of ensheathment at a time when the synapses should be fully ensheathed results in an increased number of synapses. Together these data clarify our understanding of glial process morphogenesis and its relationship to synaptic ensheathment and formation.

MATERIALS AND METHODS

Animals

All experiments were performed using C57/BL-6 mice from Charles River Laboratories or from our breeding facility. Mice were kept on regular light/dark cycles. All protocols were approved by the Brown University Institutional Animal Care and Use Committee.

Preparation and Labeling of Organotypic Cerebellar Slices

P9–P11 pups were sedated using hypothermia, and older pups (P13–P25) were anesthetized with ketamine/dormitor (70 mg/kg, 0.5 mg/kg, respectively) before rapid decapitation with sharp scissors. Brains were removed from the skulls immediately and the cerebellum was dissected out. Sagittal 300 μm cerebellar slices were prepared with a McIlwain tissue chopper or vibratome, rinsed with CMF-PBS, and cultured for 5 days *in vitro* (DIV) on MF-Millipore membranes (mixed cellulose esters, hydrophilic, 0.45 μm pore size) in Millipore-Millicell inserts (hydrophilic PTFE, 0.4 μm pore size, Fisher Scientific) in media containing 10% horse serum (Hyclone) at 37°C, 5% CO_2. Slices were transfected with DNA plasmid containing EGFP reporter gene (driven by a CMV promoter) using biolistic transfection as previously described (Dunaevsky et al., 1999) and imaged 48 h later.

Acute Slices

After allowing 48–72 h for viral expression, acute slices were prepared as described earlier. To reduce drift during imaging, slices were placed on MF-Millipore membranes for 20 min in a 37°, 5% CO_2 incubator. Although changes in spines and glia occur immediately after slice preparation, they are transient and recover within 1–2 h (Fiala et al., 2003). We therefore allowed at least 1 h for recovery time before acute slice imaging experiments.

Adenovirus Production

The GFP and the dn-Rac1 GFP adenoviruses have been previously described (Harrington et al., 2002). For the dn-RhoG adenovirus, the EcoR1 (blunted) and Not1 fragment of RhoGIP122 cDNA was first ligated into Bgl2 (blunted)-Not1 sites in pTrack-CMV (He et al., 1998). RhoGIP122 construct was a gift from A. Blangy. The recombinant adenovirus was generated in RecA+ bacteria according to He et al. (1998). The virus was purified using two rounds of CsCl centrifugation, and the CsCl was subsequently removed by dialysis.

Viral Labeling of Bergmann Glia in the Intact Animal

P11–12 and P22–P23 mice were anesthetized with ketamine/dormitor cocktail and placed in a stereotaxic apparatus. After the animal was deeply anesthetized, a small incision was made on top of the head to expose the skull. A small hole was drilled above the vermis of cerebellum with a dental drill. A glass electrode backfilled with supernatant containing GFP/adenovirus (at both ages), or N17Rac1/GFP/adenovirus (Harrington et al., 2002), or N17dn-RhoG/GFP/adenovirus was inserted into the anterior vermis at a depth of 100–700 μm, using stereotaxic equipment to judge depth. Using a picospritzer, a volume of 0.2–0.4 μL was injected over 15 min into cerebellum. Following injections, skin was sutured. Younger pups were reunited with mother, while older, self-sufficient pups were provided with food and water in their own cages. All pups were monitored regularly from the surgery until the day of imaging to ensure normal feeding and activity.

Rac1 Activity Assay

To test that dn-Rac1/GFP construct inhibits rac1 activity in our tissue, we injected either dn-Rac1/GFP adenovirus or GFP adenovirus into the cerebellum, as described earlier. After 2 days, cerebella were removed and areas with GFP fluorescence in BG were dissected out. A Rac1 activity assay was then performed on this tissue, as described in Harrington et al. (2002).

Time-Lapse Imaging of Slices and Image Analysis

Imaging was conducted using a multiphoton laser-scanning microscope Radiance 2000, BioRad coupled to a Nikon E-600-FN microscope). High-resolution imaging was performed with a long working distance, dipping

objective 60×, N.A. 1. The Millicell culture insert carrying the labeled slices was cut out and placed in the imaging chamber. Slices were perfused with oxygenated artificial cerebral spinal fluid (ACSF) at 35–37°C. For the slice cultures, we added the anti-oxidant Trolox (Sigma, 0.25 g/L) to the ACSF to decrease photodamage. Slices were held in place using a platinum and nylon harp. The imaging chamber was kept at 35–37°C (Warner Instruments). Images were collected every 30 s for a period of 15 min at a digital zoom of five (yielding a pixel size of 0.08 × 0.08 μm). At each time point, 3–7 focal planes 0.5 μm apart were collected. Although this volume included many complete spines and glial processes, we also collected an extended z-stack 5–10 μm deep before and after imaging to record the full extent of a dendritic or glial shaft. In this way, we can unequivocally determine whether structures that have appeared or disappeared during the time-lapse series are new structures or ones that entered or left the focal plane.

Drug Treatments

Before drug administration, we imaged slice cultures made from P10–11 mice for 15 min, as described earlier, to provide a baseline for comparisons to treated cells. We then bath-applied a drug and reimaged the same volume of the same glial-processes, every 30 s for 30 min, while the drug was present in the ACSF. We used the following drugs (Sigma): cytochalasin D (1 μg/mL washed in for 20 min before imaging), caffeine (1–2 mM), PPADS (25 μM), or KCl (7 mM).

Immunocytochemistry

Postnatal day (P)13–14 and P24–25 mice were perfused using 4% paraformaldeyhde. Brains were removed and postfixed overnight at 4°C in 4% paraformaldehyde, then sunk in 30% sucrose 0.1 M PB solution (1–2 days). The tissue was cast in OCT and held at −80°C until it could be sliced. At that time, the brains were equilibrated to −20°C and sectioned to 45 μm using a cryostat (Leica). Sections were kept in PBS, then floating sections were put in a blocking solution of 10% normal goat serum and 0.1% Triton X in PBS for 1 h at room temperature. Primary antibodies for s100β (Sigma, 1:250), Calbindin (SWANT, 1:400), and VGluT1 (Chemicon, 1:5,000) diluted in 1% normal goat serum and 0.1% Triton X in PBS were added to the sections and incubated either overnight at 4°C or 3 h at room temperature. Sections were rinsed in PBS and incubated in secondary antibodies conjugated with Alexa Fluor 488, 568, 594, or 647 (Molecular Probes/Invitrogen, 1:500) for 1 h at room temperature. Sections were rinsed and mounted onto slides using VectaShield mounting medium for fluorescence (Vector Laboratories, Burlingame, CA). For the development studies, slides were imaged on a Leica confocal microscope with a 63× (1.4 NA) oil objective, at a digital zoom of either one or five (yielding a size of 0.26 or 0.093 μm/pixel, respectively), with Z-steps of 1 μm or 0.2 μm, respectively. For the ensheathment studies, we imaged slices on a Zeiss LSM510 confocal microscope with a 63×, (1.4 NA) oil objective at a digital zoom of five, yielding a pixel size of 0.05 μm/pixel.

Electron Microscopy

P12 and P24 mice were perfused with 2.5% glutaraldehyde, 2.5% paraformaldeyhde, 0.1 M PB. Brains were sectioned on a vibratome at 75 μm. In some cases, floating sections containing virally labeled GFP expressing cells were incubated in blocking solution to block nonspecific binding (10% NGS, 0.1% TritonX-100 in PBS) for 1 h and incubated in polyclonal anti-GFP (Molecular Probes) in 1% NGS, 0.01% TritonX-100, (overnight at 4°C). Sections were rinsed three times in PBS (20 min) and incubated in HRP-conjugated secondary antibody (1 h, RT). Sections were exposed to diaminobenzidine (DAB, 0.15%) in Tris Buffer for 2–3 min. Sections were fixed in osmium, dehydrated, embedded in Epon, and sectioned to 10 microns. Sections were thin-sectioned to 80 nm, stained with 4% uranyl acetate in methanol followed by lead citrate, and imaged with a Philips 410 transmission electron microscope as described in (Dunaevsky et al., 2001).

Analysis of Glial Process Morphology

For all measurements, we analyzed 1–2 cells per animal, with a minimum of five animals per condition, except where noted otherwise. We processed and analyzed the data with custom-written macros using ImageJ and NIH/Scion Image. All images were blinded before analysis. We used the following analysis methods.

Density of glial appendages: The number of processes per 10 μm of glial shaft was counted in sets of seven z-stacks.

Length measurements: We measured the length of glial processes from the glial shaft to the process tip in maximal intensity projections of seven z-stacks, stepping through individual stacks when necessary to distinguish between two processes that appear to overlap in the projections (Supp. Info. Fig. 3). For branched processes, we measured to the tip of the main projection; we did not measure side branches of the process. If a process was split and the main process could not be determined, we measured the length from the shaft to the longest tip. Only processes protruding laterally were measured because of lower axial resolution.

Surface area index of glial appendages per shaft: Using ImageJ, seven z-stacks of an individual glial shaft and its processes were projected and thresholded. The image was then binarized, and all pixels within the soma and main shaft were digitally erased, leaving only the glial processes. Surface area index of the glial appendages were then measured by counting black pixels (Supplemental Fig. 4). This method provides us with

an estimation of the area of processes protruding from the shafts. We only perform this analysis on cells from slice culture labeled biolistically, as they are isolated and therefore render more accurate measurements.

Morphological categorization of glial processes: Glial processes were divided into four categories: *bulbous*, which consist of large diameter, rounded and often reticular heads attached to the shaft by a small neck; *stubby*, which are simple lateral protrusions under 2 μm long; *thin*, which are thin protrusions between 2 and 10 μm long, with no branches; and *branching*, which include any appendage which splits more than once, but still has a clear main process. We considered a process to be branching only if it was under 10 μm long and therefore not a branch of the main shaft (Fig. 2a). Processes over 10 μm that could not be differentiated from new shafts were not included in this analysis.

Ensheathment Analysis

Light level analysis

To determine the extent of spine ensheathment, we immunostained sections from P13 and P24 GFP or GFP-dn-Rac1 adenovirus injected cerebella with the Purkinje cell marker calbindin (SWANT, 1:400). We located a calbindin-labeled spine, then divided it into quadrants and determined in the color-merged image how many quadrants (1–4) of the spine were contacted by a BG process (Supp. Info. Fig. 5A–C). Calbindin-labeled dendritic spines and GFP-expressing glial processes were considered to be in close proximity and in possible contact when, in the same focal plane, (1) the green glial pixels and the red spine pixels were abutting each other with no background level pixels in between, or (2) there was an overlap between the green glial pixels and the red spine pixels in at least one focal plane. Because not every BG is labeled, we only analyzed spines contacted by a GFP labeled BG.

Ultrastructural analysis

Thin sections from P12 and P24 mice were processed and photographed at 10,400×. For each synapse, we made two measurements: the circumference of the spine that is not in contact with the presynaptic terminal (S1) and the circumference of the spine that is contact with a glial process (S2). We calculated the proportion of ensheathment as S2/S1 (Supp. Info. Fig. 5D).

Analysis of Glial Process Dynamics

Spine motility was quantified using "Motility Index" as previously described (Dunaevsky et al., 1999). In short, the motility index measures the overall displacement of a process. We first measure the area of a process at seven time points that differ the most from each other in a single time-lapse movie, then subtract the smallest area from the total projected area and divide by the average area.

Analysis of Synapse Number

Light level analysis of presynaptic puncta

Brains from mice injected with either dn-Rac1/GFP expressing adenovirus or GFP adenovirus alone were fixed and sectioned as described earlier. Sections were immunostained for calbindin and VGlut1 and imaged on a Zeiss confocal microscope (as above). Using Metamorph (Molecular Devices, Sunnyvale, CA), images were separated by color, then converted to grayscale. The VGlut1 labeling was put through a low pass filter. In stacks of 9–11 consecutive z-planes, each 4 μm apart, we created two nonoverlapping boxes of 250 × 350 and 250 × 300 pixels (rendering volumes of 600–875 μm^3), and counted individual puncta within each box. Each punctum was counted only in the plane in which it first appeared, but only if the signal to noise ratio of the punctum exceeded 2.5 in at least one plane. Puncta that were very close together were determined to be separate if two intensity peaks were identified in a line scan passing through the puncta. To normalize for volume analyzed, we divided the number of puncta per box by the total volume of that box.

Ultrastructural analysis of synapse number

Brains from mice injected with either dn-Rac1/GFP expressing adenovirus or GFP adenovirus alone were fixed, sectioned, immunostained, processed for EM, and photographed as described earlier. Areas with BG labeled with virus were identified by the appearance of the electron-dense material due to the HRP reaction product. All synapses identified by a presence of postsynaptic density and synaptic vesicles in the presynaptic terminal were counted and the average synapse number per frame was calculated.

Statistical Analysis

Data were analyzed using SPSS. We checked for normality using the Shapiro-Wilk test. Data with normal distributions were analyzed using a *T*-test. Data without normal distributions were analyzed with the Wilcoxon signed-rank test to test for main effect in paired pretreatment/posttreatment comparisons and the Mann-Whitney U test, χ^2 test, or Kruskal-Wallis test with a post-hoc Dunn's Multiple Comparisons test to test for main effect in all other cases.

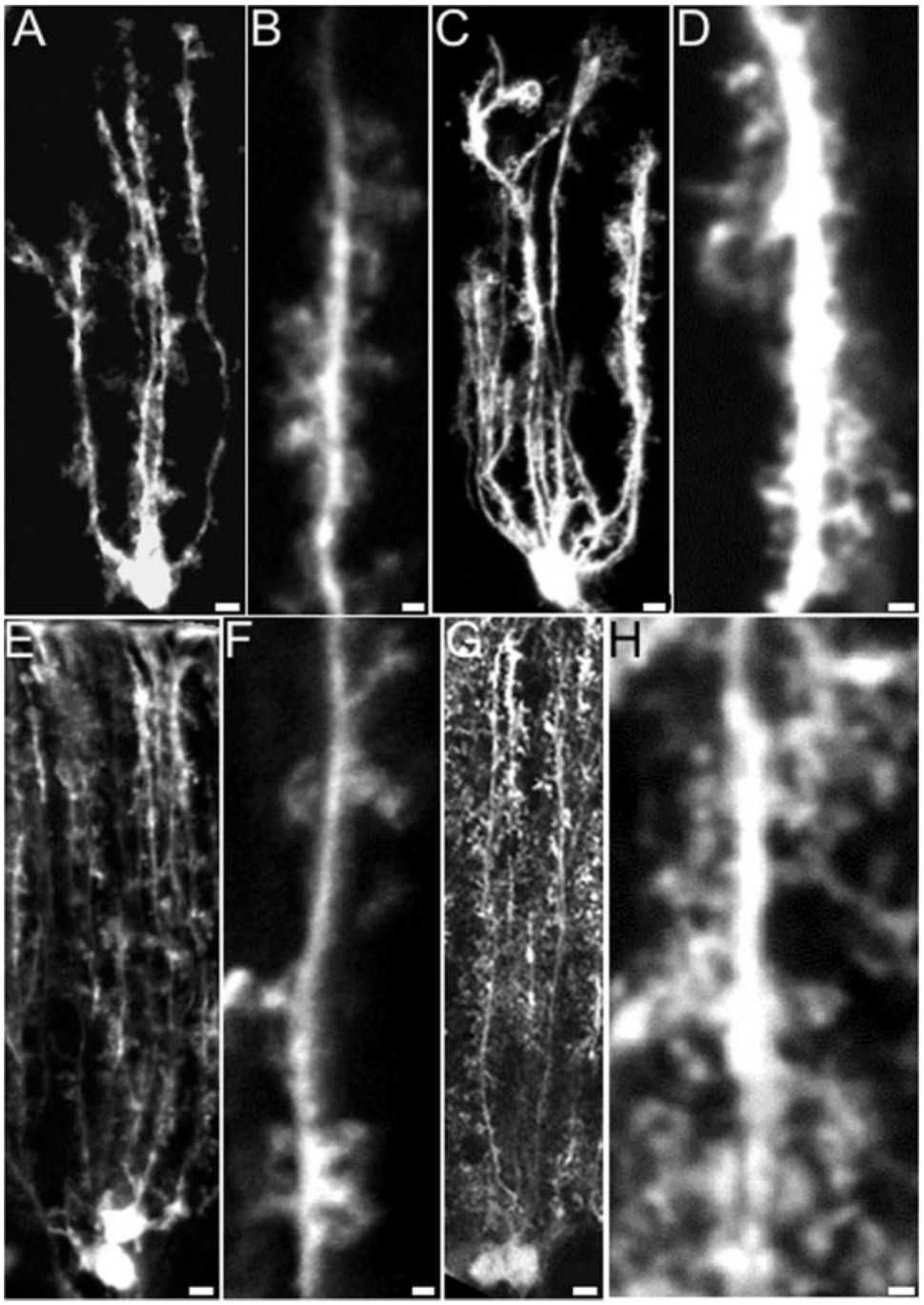

Fig. 1. Bergmann glia in organotypic and acute cerebellar slices. **A, B**: GFP-labeled BG in a P10 + 5DIV organotypic slice culture. **C, D**: GFP-labeled BG in a P20 + 5DIV organotypic slice culture. **E, F**: GFP-adenovirus-labeled BG in an acute slice from a P13 mouse. **G, H**: GFP-adenovirus-labeled BG in an acute slice from a P25 mouse. Bars: 1 μm (A, C, E, and G), 5 μm (B, D, F, and H).

RESULTS

Labeling and Identification of Bergmann Glia and Their Processes

Bergmann glia are readily recognizable by their morphology (see Fig. 1) and orientation in the cerebellar cortex. We used the following criteria to visually define cells as Bergmann glia: (1) 3–6 thick radial shafts extending through the molecular layer to the pial surface, (2) small cell body in the PC layer, (3) end-feet that contact the pial surface, (4) small protrusions extending from the major glial cell shafts ("microdomains"; Grosche et al., 1999), and (5) lack of an axon. Staining with the glial marker s100β confirmed our morphological assessment (Supp. Info. Fig. 1). Because we are labeling cells with cytosolic GFP, we were concerned that fine Bergmann glia processes containing little cytoplasm might not be detected. We therefore coexpressed a cyto-

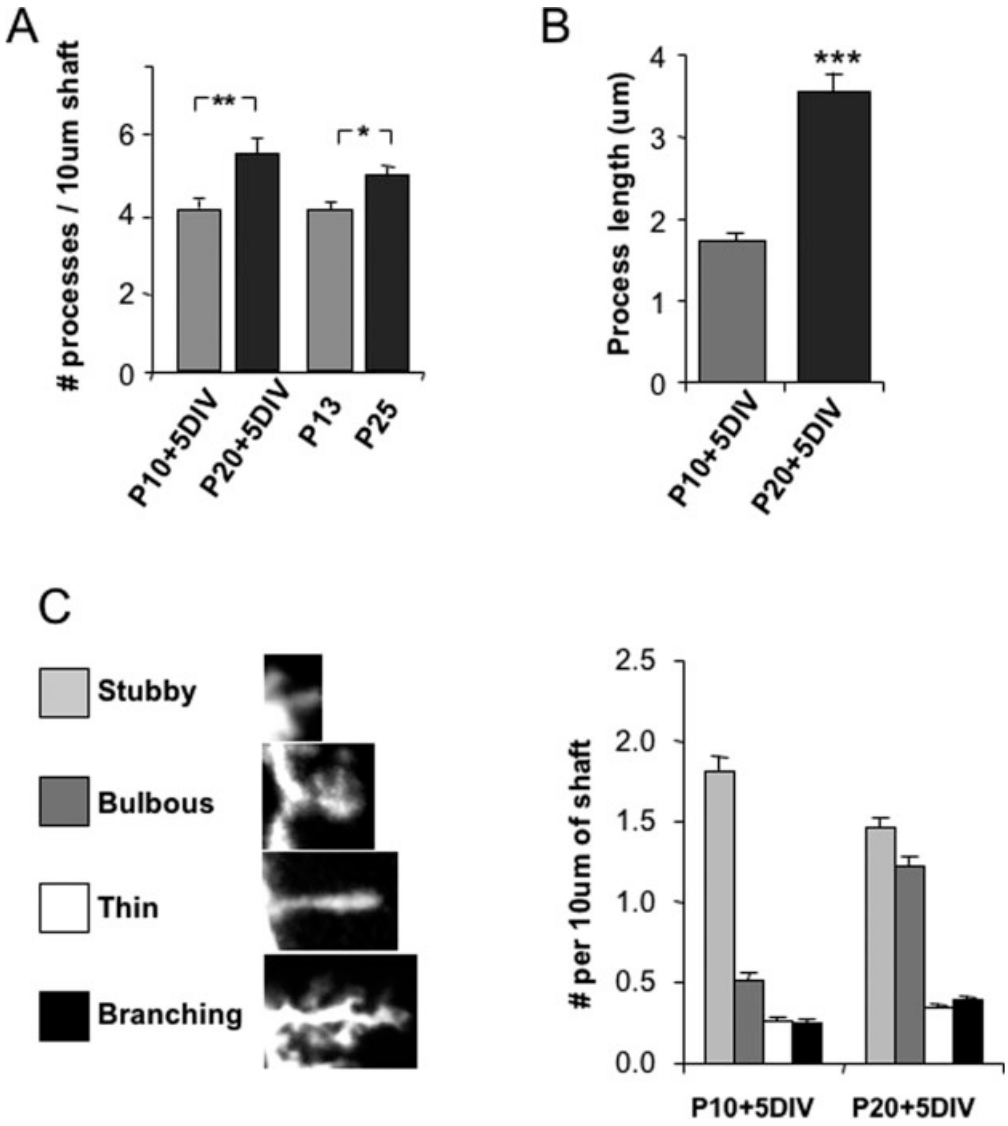

Fig. 2. Developmental changes in BG process morphology. **A**: The density of BG processes increases significantly with age in both slice culture and acute slices. **B**: The length of BG processes increases significantly with age in organotypic slice cultures. **C**: Distribution of the four most common process morphologies (stubby, bulbous, thin, and branching) observed in BG at P10 + 5DIV P20 + 5DIV slice cultures.

solic fluorescent protein, tdTomato, with membrane-targeted (farnesylated) GFP (GFP-f) in BG from P11 + 7DIV slice cultures. Since both markers labeled the processes to a similar degree (Supp. Info. Fig. 2), we concluded that we are in fact visualizing the extent of glial processes with cytosolic GFP.

Development of Bergmann Glial Processes

We examined the morphology of BG at two developmental stages, early and late in synaptogenesis (P9–P11 and P18–P20). After biolistically labeling cells from slice cultures (5DIV), we examined labeled BG using two-photon microscopy (Fig. 1A–D). The BG from the older group of animals had a 25% higher density of processes than those of the younger group (Fig. 2A; $P = 0.002$, Mann Whitney U Test, $n = 17/17$ shafts from 12/9 cells for P10/P20). We did not include in our analysis processes extending into external granule layer and outer molecular layer near BG end feet because at P10 BG shafts lack the small protrusions studied here (Rakic, 1971; Yamada et al., 2000). To confirm the cultured slice results, we also analyzed cells in acute cerebellar slices following *in vivo* labeling of young (P11–12) and older (P22–23) mice with GFP expressing adenovirus (Fig. 1E–H, Fig. 3A), which preferentially labels glial cells when injected into the molecular layer of the cerebellum. As seen in the cultured slices, glia process density in the acute slices increased 22% from second to third postnatal weeks (Fig. 2A; $P = 0.014$, Mann Whitney U Test, $n = 21/16$ shafts from 14/10 cells from P13/P26).

In addition to an increase in the density, the length of the BG processes in slice cultures doubled over this time

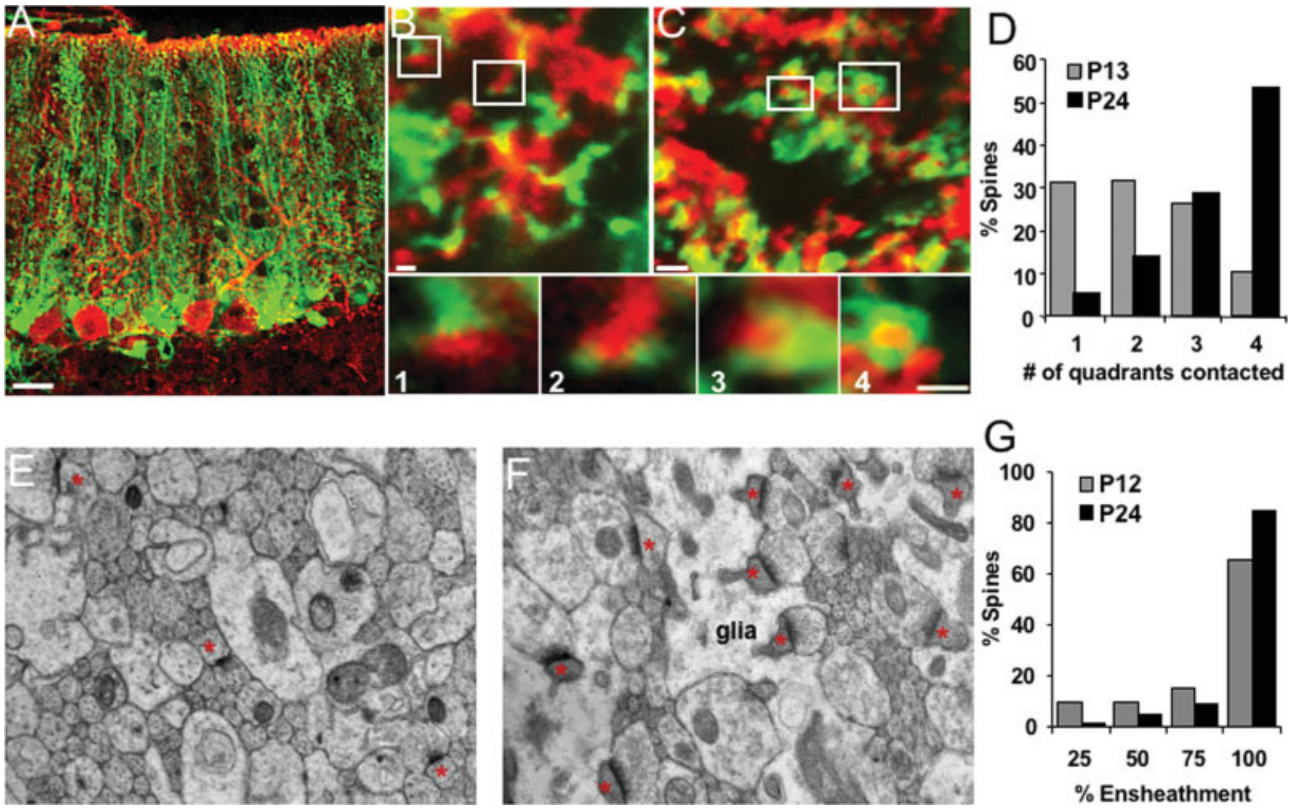

Fig. 3. Developmental increase in ensheathment of PC dendritic spines by BG processes. (**A**) Purkinje cells immunostained with calbindin (red) in acute slice from GFP-adenovirus injected mouse. Glial ensheathment grows more complete between P13 (**B**) and P24 (A, **C**). High magnification images from B and C are labeled with numbers indicating how many quadrants of the red spine are contacted by a green BG process (1–4). Glial ensheathment of spines is quantified in (**D**), by measuring quadrants of the spine that were in contact with a GFP-labeled BG. **E**: Electron micrographs of the cerebellar molecular layer from P12 (E) and P24 (**F**) mice. Note that synapses (red asterisks) are more fully ensheathed by glial processes (glia) in the older animals. Glial ensheathment of spines is quantified in (**G**). Bar: 20 μm (A), 1 μm (B) 4.2 μm (C), and 500 nm (E, F). For high magnifications of B and C, the bar in box 4 = 0.75 μm (3) and 1 μm (1,2,4). [Color figure can be viewed in the online issue, which is available at www.interscience.wiley.com.]

period (Fig. 2B; $P < 0.0001$, Mann Whitney U Test, $n = 211$ processes from 6 cells for P10, $n = 113$ processes from six cells for P20). To obtain a more specific view of how the processes changed over time, we determined the frequency of the most common process shapes. Many processes fell into one of the following categories: stubby, bulbous, thin, and branching (Fig. 2C). Although all of the morphologies were present at both ages, the more complex and reticular bulbous processes became prevalent in older animals ($P = 0.01$, χ^2, $n = 10$ cells for P10 and 11 cells for P20). Because not every process fit into one of these four morphologies, the category analysis represents only a subset of stereotypical processes. Because of this, we measured the Surface Area Index, an additional measure of process complexity. The Surface Area Index allows us to obtain a general area measurement of all the processes protruding laterally from the shaft including those without stereotypical shapes and those that were too close to be easily resolved and measured using our other parameters. We found that this index also increased with development (Supp. Info. Fig. 4, $P = 0.025$, Mann Whitney U Test, $n = 31$ shafts from 11 cells for P10, $n = 37$ shafts from nine cells for P20). Therefore, a substantial glial process expansion occurs during the second and third postnatal weeks, a period of extensive synaptogenesis.

Ensheathment of PC Dendritic Spines Increases with Age

Glial cells ensheath synapses in the hippocampus, cortex, and cerebellum (Grosche et al., 1999; Peters et al., 1976; Spacek, 1985; Ventura and Harris, 1999). To ask how BG process development relates to synaptic ensheathment, we imaged the PC and BG together early and late in synaptogenesis using multi-channel confocal imaging. We stained sections with dense GFP-labeled BG from P12–14 and P24–25 mice with the PC-marker calbindin (Fig. 3A–C). We divided individual PC spines into quadrants and scored how many quadrants were in contact with a glial process, thus quantifying the level of BG process coverage for each spine (Fig. 3, Supp. Info. Fig. 5A–C). BG from older mice covered the spines more completely than those from younger mice, indicating a developmental increase in ensheathment (Fig. 3D, $P < 0.0001$, χ^2 test, $n = 232/313$ spines from 4/4 animals from P13/P24 mice). Since it is possible that some spines

are contacted by unlabeled glial cells we have performed a similar ensheathment analysis on the ultrastructural level. Electron micrographs of the molecular layer from randomly chosen thin sections were analyzed (Fig. 3E,F). Ensheathment of spines was computed and compared between sections from P12 and P24 mice (Supp. Info. Fig. 5D). Similar to the light level analysis, we found that glia more completely surround spines in older mice than in younger mice (Fig. 3G, $P < 0.0001$, χ^2 test, $n = 581/981$ spines, $n = 55/56$ fields, from 3/3 animals from P12/P24 mice). These findings demonstrate that increases in glial process number, length, and complexity over development correlates temporally with increased ensheathment of synapses.

Motile Glial Processes

During development dendritic spines are surprisingly motile. Since Purkinje cell dendrites and their spines develop in concert with glial processes (Lordkipanidze and Dunaevsky, 2005; Yamada et al., 2000), we examined the dynamic properties of BG processes with time-lapse imaging. We found that the processes are also highly dynamic, displaying many of the same types of motility as spines: formation of new processes as well as growth, retraction, and morphing of existing glial processes (Fig. 4, Supp. Info. Movie 1A).

We next determined whether BG process motility is developmentally regulated. Using a motility index (MI) to measure the process dynamics in cultured slices (Dunaevsky et al., 1999), we found that BG process motility decreases by 63% in older cells (Fig. 4E; $P < 0.0001$, Mann Whitney U Test, $n = 47/42$ processes from 7/8 cells for P10/P20). Although a developmental shift in glial process categories (Fig. 2C) might contribute to reduced motility in older cells, there was a clear reduction in motility within the categories in older cells (Supp. Info. Fig. 6).

Glial process dynamics have been reported only in organotypic slice culture (Benediktsson et al., 2005; Haber et al., 2006; Nishida and Okabe, 2007). To determine whether glial process motility occurs in more physiologically relevant model, we imaged acute slices from cerebella labeled with GFP using an adenoviral vector *in vivo*. While the baseline motility in the processes from Bergmann glia was lower than in cells from slice cultures, the developmental pattern of the process dynamics persisted, decreasing by 57% in the late stage of cerebellar synaptogenesis (Fig. 4C–E; $P < 0.0001$, Mann Whitney U Test, $n = 37/32$ processes from 8/4 P13/P26 cells). Thus, similar to the dendritic spines they ensheath, BG side processes are dynamic and their motility is developmentally regulated.

Mechanisms Regulating BG Process Motility

Actin polymerization is known to regulate cellular morphology and process motility, including that of dendritic spines (Dunaevsky et al., 1999; Fischer et al., 1998). To find whether actin polymerization was necessary for BG process motility we treated P10 + 5DIV slice cultures with 1 μg/mL cytochalasin D (cyt D), an inhibitor of actin polymerization. In the presence of the drug, motility of BG processes significantly decreased (Fig. 5A–C, Supp. Info. Movie 2), as compared with the same processes before treatment ($P = 0.0003$, Wilcoxon Signed-Rank Test, $n = 25$ of processes from three cells). Thus, actin polymerization is necessary for glial process dynamics.

BG respond to neurotransmitter release and depolarization by an increase in intracellular calcium (Grosche et al., 1999). Calcium may influx through membrane receptors, such as the P2 purinergic receptors (Piet and Jahr, 2007), and by release of calcium from internal stores. We next set out to determine if these factors regulate glial process motility. General depolarization with elevated potassium chloride (KCl) did not significantly affect process motility (Fig. 5D, $P = 0.40$, Wilcoxon Signed-Rank Test, $n = 25$ processes from five cells). Blocking P2 purinergic receptors with 4-[[4-Formyl-5-hydroxy-6-methyl-3-[(phosphonooxy)methyl]-2-pyridinyl] azo]-1,3-benzenedisulfonic acid tetrasodium salt (PPADS) also did not alter glial process motility (Fig. 5E, $P = 0.09$, Wilcoxon Signed-Rank Test, $n = 21$ processes from five cells). Although blocking these surface receptors did not change motility, causing a general release of calcium from glial cell internal stores by bath application of 2 mM caffeine did decrease BG process motility (Fig. 5F, $P = 0.0013$, Wilcoxon Signed-Rank Test, $n = 30$ processes from six cells). We therefore conclude that neither depolarization of the BG nor subsequent entry of calcium through P2 receptors alone regulates process motility, but that release of intracellular calcium is sufficient to reduce glial process dynamics.

Rac1 and RhoG Regulate Glial Process Length

Small GTPases such as Rac1 and RhoG have been implicated in rearrangement of the actin cytoskeleton in cellular processes including dendritic spines (Nishida and Okabe, 2007; Tashiro and Yuste, 2004). Since both Rac1 and RhoG are expressed in the molecular layer of the cerebellum (O'Kane et al., 2003) we examined their role as potential regulators of BG morphology and motility. The dominant-negative (dn) forms of Rac1 (Harrington et al., 2002) and RhoG compete with endogenous Rac1 and RhoG for binding sites on guanine exchange factor (GEF), preventing these GTPases from entering their active, GTP-bound form. We introduced dn-Rac1/GFP, dn-RhoG/GFP, or GFP alone *in vivo* into BG of P11–P12 mice. After 2 days, we imaged the GFP-labeled BG in acute slices (Fig. 6A–F). At this time point, we see a decrease in active Rac1 because of the injection of dn-Rac1 adenovirus (Supp. Info. Fig. 7). In contrast to reports for hippocampal astrocytes (Nishida and Okabe, 2007), we did not observe a difference between the motility of the processes expressing either dn-Rac1

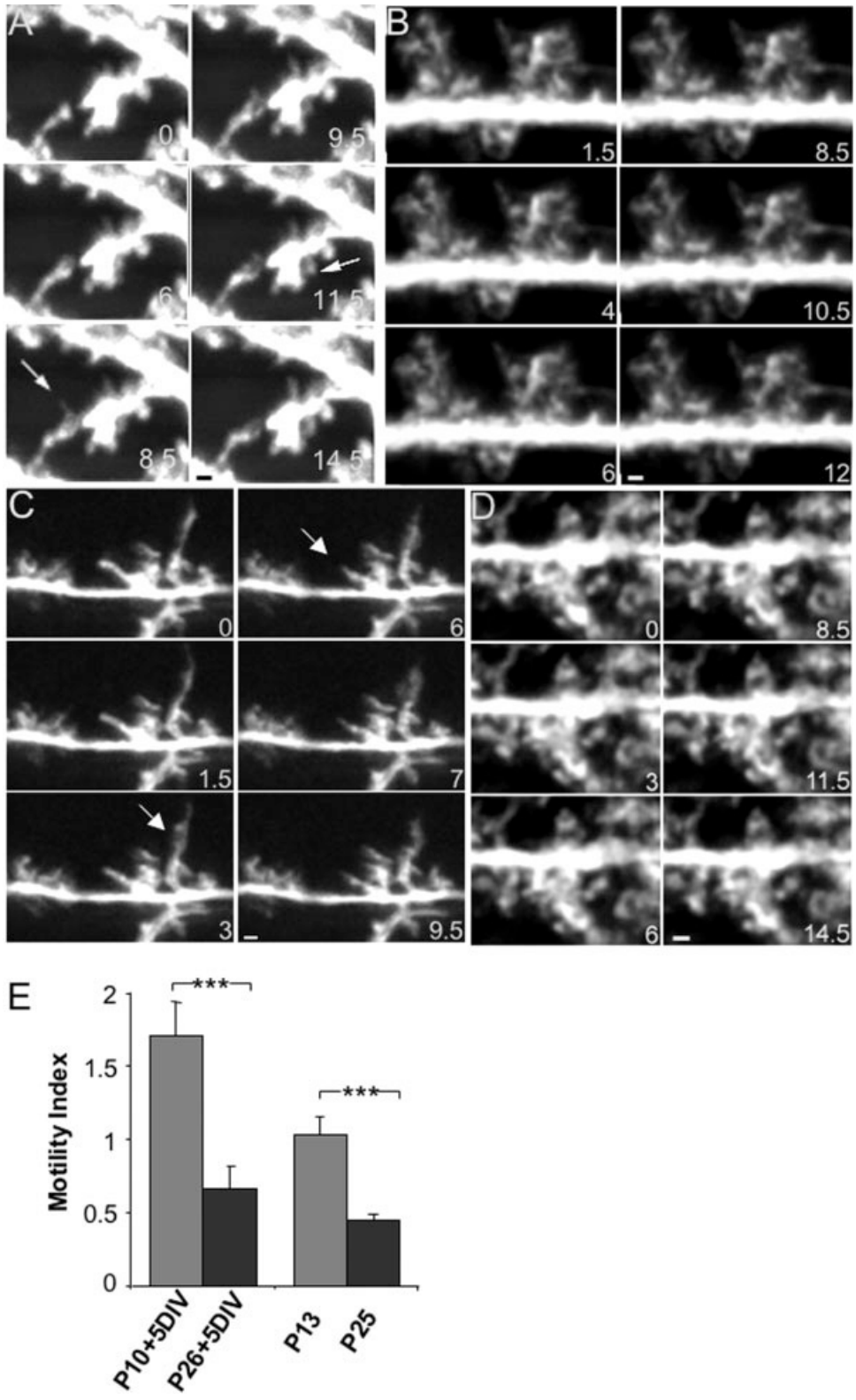

Fig. 4. Developmental decrease in BG process motility. Time-lapse images of GFP-labeled BG in P10 + 5DIV (**A**) and P20 + 5DIV (**B**) organotypic slice cultures and GFP-adenovirus transfected BG in P13 (**C**) and P25 (**D**) acute slices. Arrows point to motile processes. Time is indicated in minutes. Bar = 1 μm. See supporting information for movies. (**E**) Motility decreases with development in both slice cultures and acute slices.

(n = 21 processes from 10 cells) or RhoG (n = 22 processes from seven cells) compared with controls (n = 37 processes from eight cells, Fig. 6I, P = 0.6463, Kruskal-Wallis test). In addition, neither dn-Rac1 nor dn-RhoG expression altered the density of BG processes (Fig. 6G, P = 0.116, Kruskal-Wallis test, n = 32/25/27 shafts from 19/21/23 dn-Rac1/dn-RhoG/control cells). However, expression of either dn-Rac1 or dn-RhoG significantly

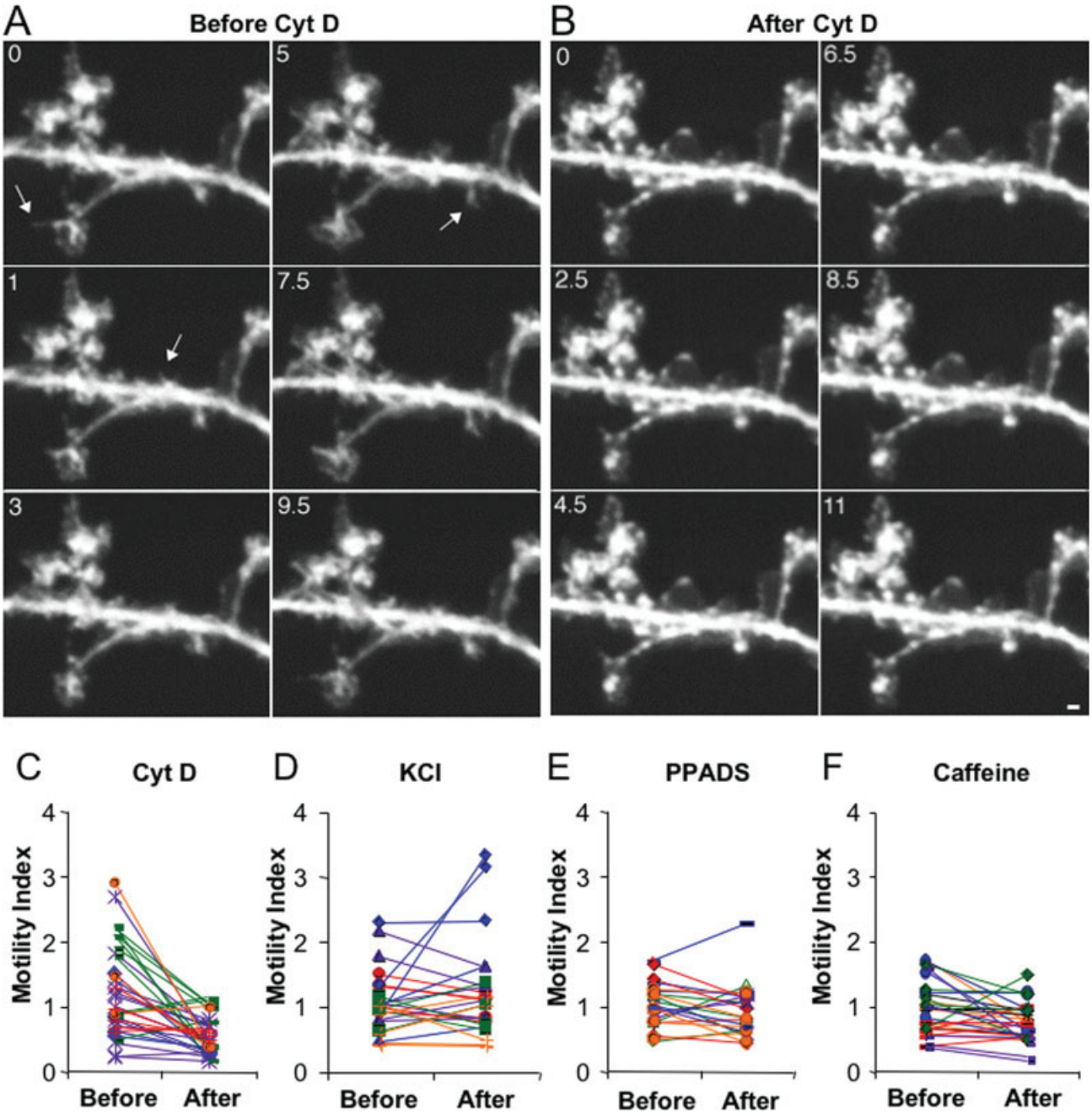

Fig. 5. Regulation of Bergmann glial process dynamics. Time-lapse images of a GFP-labeled BG from P10 + 5DIV slice culture before (**A**) and (**B**) after bath application of 1 μg/μL cytochalasin D. Arrows point to motile processes. Time is indicated in minutes. Bar = 1um. (**C**) MI of individual processes before and after cytochalasin D treatment demonstrating the decreased motility after treatment. There is no overall change in MI of individual processes before and after treatment with KCl (**D**) or PPADS (**E**), but caffeine causes a significant decrease in MI (**F**). (C–F) Color of the line indicates the cell containing each process. [Color figure can be viewed in the online issue, which is available at www.interscience.wiley.com.]

decreased the lengths of processes by 23% and 27%, respectively, as compared with controls (Fig. 6H, $P < 0.0001$, Kruskal-Wallis test, $n = 190/286/147$ processes from 10/17/7 dn-Rac1/dn-RhoG/control cells). Thus, Rac-1 and Rho-G (which can act through the Rac-1 pathway) regulate the morphogenesis but not the dynamics of BG processes.

Decreased Process Length Results in Decreased Glial Coverage of Spines

To link the outgrowth of glial processes with synapse ensheathment, we analyzed spine ensheathment in animals injected with GFP-dn-Rac1 virus. Expression of dn-Rac1 in P20 animals for 2 days caused a 22% reduction

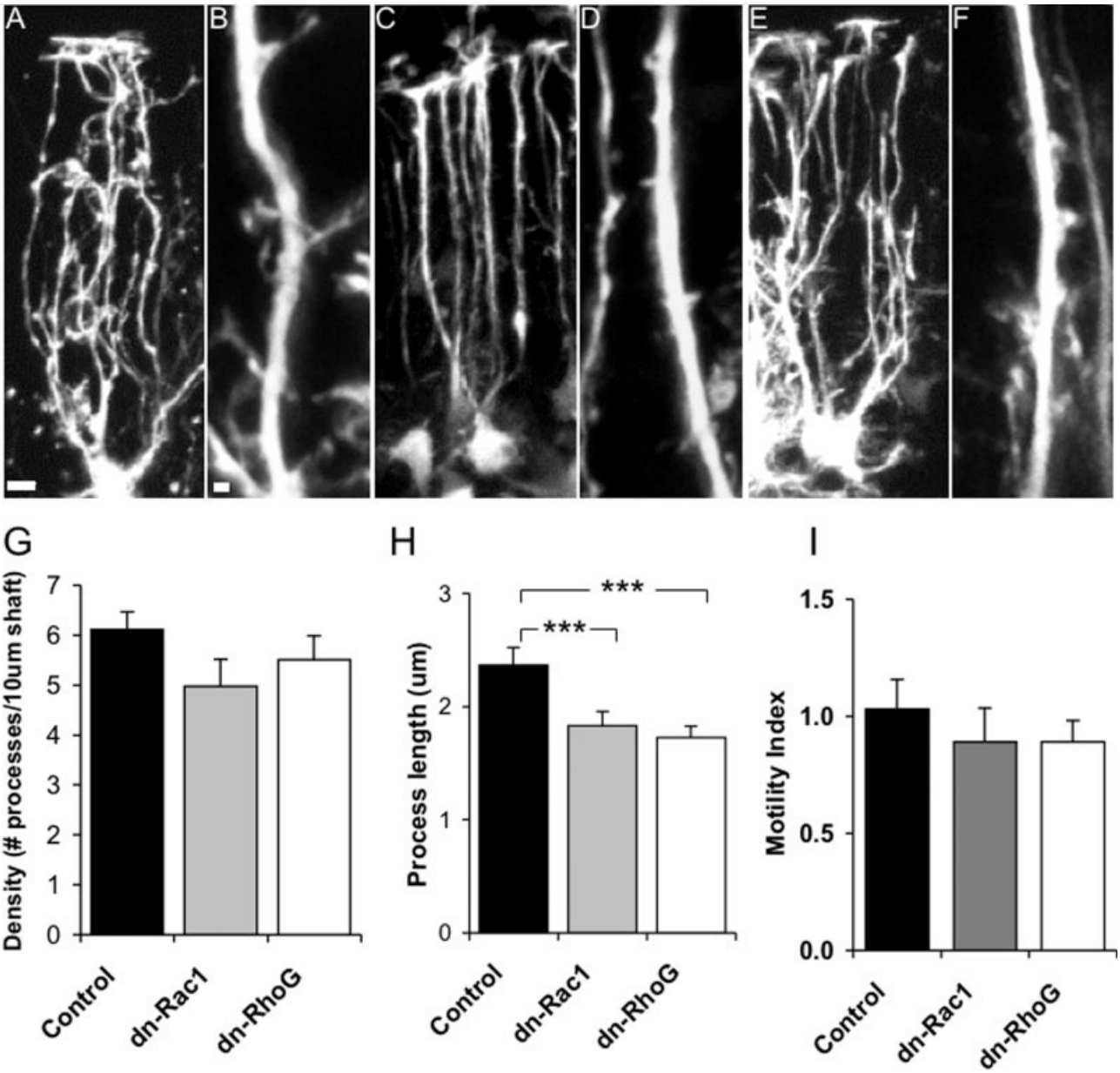

Fig. 6. Rac1 and RhoG reduce BG process length. BG from P14 acute slices expressing GFP (**A, B**), dn-Rac1/GFP (**C, D**), or dn-RhoG/GFP (**E, F**). Measurements of density (**G**), length (**H**), and motility (**I**) of the processes, demonstrating that only process length is significantly affected by blocking Rac1 or RhoG activity in the BG. Bar: 1 μm (A, C, E), 5 μm (B, D, F).

in glial process length compared to control cells (Fig. 7A, $P = 0.001$, Mann-Whitney U test, $n = 119$ processes from seven control animals and 137 processes from five dn-Rac1 animals). Importantly, dn-Rac1 expressing BG ensheathed dendritic spines to a lesser degree than control cells (Fig. 7B,C, $P = 0.002$, χ^2 test, $n = 774$ spines from seven control animals and 792 spines from five dn-Rac1 animals). Thus glial process expansion during development is linked to Purkinje cell synapse ensheathment in the cerebellum.

Decreased Ensheathment Correlate With an Increase in Synapse Number

To examine the role of ensheathment at the synapse, we used dn-Rac1 to decrease the level of ensheathment, and then counted the subsequent number of synapses. We immunostained sections from GFP and dn-Rac1/GFP-adenovirus injected P24 mice with calbindin and the presynaptic marker VGluT1. Areas with clear GFP expression (labeled glia) were chosen for imaging and

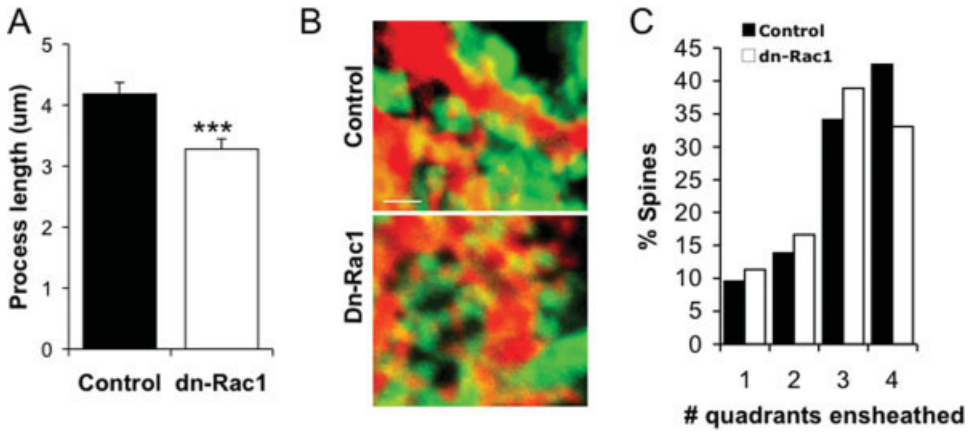

Fig. 7. Decreased process length correlates with decreased coverage of dendritic spines in P24 mice. (**A**) BG in P24 mice expressing dn-Rac1 and GFP are an average of 22% shorter than BG expressing GFP alone (**B**). The shorter processes in the BG expressing dn-Rac1 (bottom) cover the spines less completely than processes from control mice, as quantified in (**C**). Bar = 1 μm. [Color figure can be viewed in the online issue, which is available at www.interscience.wiley.com.]

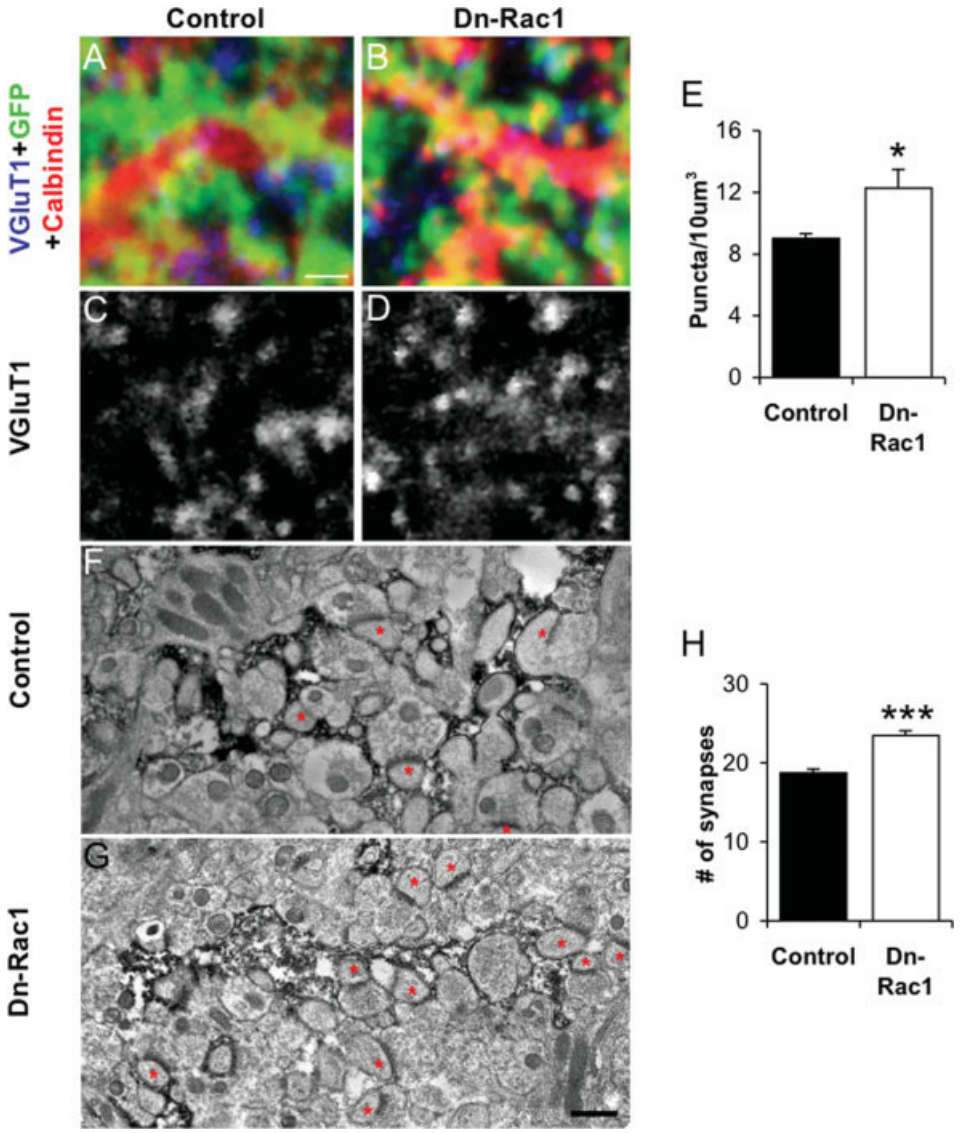

Fig. 8. Synapse number in P24 mice with reduced ensheathment. (**A**) Confocal images of BG (green) expressing GFP alone or dn-Rac1 and GFP (**B**) in sections immunostained with PC marker calbindin (red) and presynaptic marker VGluT1 (blue). (**C, D**) VGluT1 staining from (A) and (B), respectively. (**E**) Decreasing the level of glial ensheathment with dn-Rac1 increases the number of VGluT1 puncta. (**F**) Electronmicrographs of the molecular layer from mice with BG expressing GFP alone or dn-Rac1 and GFP (**G**). GFP expressing BG are identified by presence of the dark HRP reaction product. Note a larger number of synapses (red asterisks) in mice expressing dn-Rac1 and GFP. (**H**) Average number of synapses increases in mice with BG expressing dn-Rac1 and GFP. Bars in (A) and (C) = 1 μm; Bar in (G) = 0.5 μm. [Color figure can be viewed in the online issue, which is available at www.interscience.wiley.com.]

presynaptic puncta analysis (Fig. 8A,B). Surprisingly, we found 27% more VGluT1 puncta in sections with BG expressing dn-Rac1 (Fig. 8A–E, $P = 0.014$, Mann Whitney U Test, $n = 8$ z-stacks (5,251 puncta in total volume of 5,850 μm^3) from four GFP-injected mice and $n = 8$ z-stacks (7,664 puncta in total volume of 6,337.5 μm^3) in three GFP-dn-Rac1 injected mice). Since we only counted presynaptic terminals, we next performed a similar analysis on the ultrastructural level. Regions containing virally labeled BG were identified by the appearance of electron dense material following immunostaining against GFP (Fig. 8F,G). In agreement with the light level analysis, we counted 25% more synapses in dn-Rac1 expressing animals (Fig. 8F–H, $P < 0.001$, Mann Whitney U Test, $n = 99$ frames in three animals for each condition. Taken together, these experiments show that there are more presynaptic terminals and full synapses present when the glial sheath does not fully surround the spine.

DISCUSSION

Bergmann glial (BG) surface area expands by an estimated 50-fold during the first 3 weeks of a mouse's life (Grosche et al., 2002), after which most excitatory synapses in the cerebellar cortex are ensheathed by BG. How glial processes develop and subsequently ensheath synapses is not well understood. Here we examined how process expansion and ensheathment occur, as well as the dynamic nature of processes as they grow. We find that density and complexity of BG processes increase over the period of synaptogenesis, and that increased outgrowth of glial processes is correlated with proper ensheathment of dendritic spines. Moreover, experimentally reducing ensheathment leads to a greater number of synapses. Time-lapse imaging reveals that BG processes are highly motile early in synaptogenesis, but motility wanes in older cells. This motility is dependent on actin polymerization and intracellular calcium levels. However, cytoskeletal regulators Rac1 and RhoG do not regulate BG process dynamics or density, although they maintain process length. Our results demonstrate developmental and molecular regulation of BG process growth and dynamics, and provide important links between the expanding structure of the BG, its ability to ensheath a synapse, and the functional significance of ensheathment.

Our studies of glial process outgrowth expand upon previous examinations of BG process morphology and their association with PC (Grosche et al., 1999, 2002; Lordkipanidze and Dunaevsky, 2005; Rakic, 1971; Yamada et al., 2000) while focusing solely on time points most relevant for synapse formation and maintenance. We find extensive BG process growth during the second and third postnatal weeks, with changes in process density, length, and complexity. The different glial process morphologies could mediate different interactions with spines. Small simple processes would interact with fewer spines while more complex processes could potentially ensheath larger groups of spines. These large, multisynapse-covering processes likely constitute electrically isolated microdomains which create small functional units by synchronizing groups of synapses while isolating them from neighboring synapses (Grosche et al.,1999, 2002).

In addition, process expansion would enable glial processes to fully cover each synapse. Indeed, we find that increased outgrowth of BG processes correlates temporally with increased ensheathment of PC dendritic spines. Taking advantage of the high resolution of electron microscopy and the ability to easily gather large image stacks from light level analysis, we see that, late in synaptogenesis, almost all spines are completely enveloped by a BG process. Moreover, dn-Rac1 expression-induced shortening of BG processes resulted in only partially ensheathed spines. This directly demonstrates for the first time that BG process outgrowth is linked to proper synaptic ensheathment.

Early in synaptogenesis, BG processes, like the dendritic spines they ensheath, are highly dynamic. Here we demonstrate that BG processes rapidly grow, retract, and move laterally. Our data offer the first example of motile glial processes in acute slices and provide a direct comparison of that motility in slice cultures. Interestingly, processes of cultured BG show higher baseline motility than those from acute slices, potentially because of altered connectivity seen in organotypic cultures (De Simoni et al., 2003). We took care to avoid potential artifacts of the cells' exposure to adenovirus. We allowed 2–3 days for viral expression, at which point we saw no signs of toxicity, and did not image beyond that window. The similarity between results from injected animals and biolistically labeled slices in culture argues against major artifacts induced by viral infection.

Similar dynamics of processes, in terms of tempo and types of motility, also occur in astrocytes from hippocampal (Benediktsson et al., 2005; Haber et al., 2006; Nishida and Okabe, 2007) and brain stem (Hirrlinger et al., 2004) slice cultures. The presence of motile glial processes in multiple brain areas denotes an important, conserved purpose for this dynamic behavior, but its function remains unclear. Is glial process motility during ensheathment development a byproduct of process growth and expansion, or is it more analogous to spine motility, moving to search out a target? To investigate function, we examined how glial process dynamics are regulated.

Our study provides the first evidence that glial process dynamics are developmentally regulated, with reduced motility in older cells. This reduction of BG process motility at a time when spine ensheathment is almost complete suggests that motility may be involved in ensheathment. Haber et al. (2006) saw no change in dynamics between hippocampal astrocytes with increasing times in culture. Although developmental changes early and late in synaptogenesis may not be recapitulated in organotypic cultures, this could indicate a functional difference between cerebellar BG and hippocampal astroglia.

BG process dynamics are not activity-dependent, as neither chemically mimicking neuronal activity nor blocking its effects on glia affected motility. Local depolarization increases intracellular calcium in BG through activation of P2 purinergic receptors (Piet and Jahr, 2007), but we found that blocking these receptors does not alter process motility. Adding caffeine to the bath decreases BG process motility, indicating that calcium released from internal stores may stabilize BG processes. As caffeine also affects other aspects of cell functioning, like cAMP signaling, future experiments are necessary to determine if intracellular calcium store release is the predominant mechanism by which caffeine alters BG process motility.

We have also established that, like dendritic spines (Dunaevsky et al., 1999; Fischer et al., 1998) and hippocampal astrocytes (Haber et al., 2006), BG process motility is controlled by actin filament polymerization. Decreased glial process motility is unlikely to be a mere consequence of decreased spine motility, as all forms of BG process dynamics decrease, including emergence and retraction, after blocking actin polymerization. These forms of motility cannot be explained readily by PC spine movement, and therefore are probably directly affected by reduced actin polymerization within glial cells. Rac1, a small GTPase commonly associated with actin rearrangement, is involved in actin-dependent dendritic spine motility (Tashiro and Yuste, 2004) and hippocampal astrocyte motility (Nishida and Okabe, 2007). In contrast, expression of dominant-negative forms of Rac1 or RhoG in BG resulted in as many motile processes as in controls. We did find a role for Rac1 in BG morphogenesis, since blocking Rac1 decreases process length and synaptic ensheathment. Consistent with evidence that RhoG maybe be acting via a Rac1 pathway (Blangy et al., 2000), we found that blocking RhoG activity also decreases length without affecting motility. Perhaps, two distinct pathways, one RhoG/Rac1-dependent and one utilizing a still-unknown regulator protein, could control process length and dynamics, respectively, in BG processes.

Our findings that decreased BG process motility, increased process complexity, and increased ensheathment correlate temporally with the end of synaptogenesis, suggest a role for glial ensheathment in regulation of synaptogenesis. Indeed, we show by using both light level and ultrastructural analyses, that decreasing ensheathment levels near the end of synaptogenesis results in a higher number of synapses than in controls. This suggests that, in the cerebellum, complete synaptic coverage by glia may serve as a cap for synaptogenesis. In this model, reducing ensheathment would either revert the cells to a less mature state that supports formation of new synapses or reduces synaptic pruning. Consistent with our findings at predominantly parallel fiber synapses (as indicated by VGluT1 immunostaining), removal of glial ensheathment by overexpressing the AMPA receptor GluR2 subunit in BG results in residual multiple climbing fiber innervation of PCs (Iino et al., 2001).

Which molecular mechanisms allow for the regulation of synapse number by glial processes? Although many studies implicate glia-released soluble factors in early synaptogenesis (Ullian, 2001, etc.), the close apposition of glial processes to dendritic spines required to keep synaptogenesis at bay in our study implicates interactions of membrane-associated molecules. A likely candidate would be interaction between the Eph-Receptor tyrosine kinase and the ephrin ligand. Work in the hippocampus demonstrates that the EphA4 receptor on pyramidal neurons interacts with the glial membrane ligand ephrin-A3 to modulate dendritic spine shape and density (Murai et al., 2003; Nestor et al., 2007; Nishida and Okabe, 2007; Thompson, 2003). Although major differences exist between hippocampal and cerebellar ensheathment of synapses, if similar Eph/ephrin interactions occur in the cerebellum, this could be a viable mechanism by which the glial processes, when completely surrounding a spine, could inhibit formation of new synapses or promote synaptic pruning. It will be critical in the future to elucidate the molecular mechanism by which glial ensheathment of synapses regulate synapse formation.

ACKNOWLEDGMENTS

Carol Mason and Kimberly Harms for helpful comments on the manuscript; Chavvy Tep for the Rac1 activity assays; Whitehall Foundation and NINDS (1R01NS057667)

REFERENCES

Altman J. 1972. Postnatal development of the cerebellar cortex in the rat. II. Phases in the maturation of Purkinje cells and of the molecular layer. J Comp Neurol 145:399–464.

Amateau SK, McCarthy MM. 2002. Sexual differentiation of astrocyte morphology in the developing rat preoptic area. J Neuroendocrinol 14:904–910.

Araque A, Parpura V, Sanzgiri RP, Haydon PG. 1998. Glutamate-dependent astrocyte modulation of synaptic transmission between cultured hippocampal neurons. Eur J Neurosci 10:2129–2142.

Benediktsson AM, Schachtele SJ, Green SH, Dailey ME. 2005. Ballistic labeling and dynamic imaging of astrocytes in organotypic hippocampal slice cultures. J Neurosci Methods 141:41–53.

Blangy A, Vignal E, Schmidt S, Debant A, Gauthier-Rouviere C, Fort P. 2000. TrioGEF1 controls Rac- and Cdc42-dependent cell structures through the direct activation of rhoG. J Cell Sci 113: 729–739.

Christopherson KS, Ullian EM, Stokes CC, Mullowney CE, Hell JW, Agah A, Lawler J, Mosher DF, Bornstein P, Barres BA. 2005. Thrombospondins are astrocyte-secreted proteins that promote CNS synaptogenesis. Cell 120:421–433.

De Simoni A, Griesinger CB, Edwards FA. 2003. Development of rat CA1 neurones in acute versus organotypic slices: Role of experience in synaptic morphology and activity. J Physiol 550:135–147.

Dunaevsky A, Blazeski R, Yuste R, Mason C. 2001. Spine motility with synaptic contact. Nat Neurosci 4:685–686.

Dunaevsky A, Tashiro A, Majewska A, Mason C, Yuste R. 1999. Developmental regulation of spine motility in the mammalian central nervous system. Proc Natl Acad Sci USA 96:13438–13443.

Fiala JC, Kirov SA, Feinberg MD, Petrak LJ, George P, Goddard CA, Harris KM. 2003. Timing of neuronal and glial ultrastructure disruption during brain slice preparation and recovery in vitro. J Comp Neurol 465:90–103.

Fischer M, Kaech S, Knutti D, Matus A. 1998. Rapid actin-based plasticity in dendritic spines. Neuron 20:847–854.

Ge WP, Yang XJ, Zhang Z, Wang HK, Shen W, Deng QD, Duan S. 2006. Long-term potentiation of neuron-glia synapses mediated by Ca2+-permeable AMPA receptors. Science 312:1533–1537.

Gerlai R, Wojtowicz JM, Marks A, Roder J. 1995. Overexpression of a calcium-binding protein, S100 beta, in astrocytes alters synaptic plasticity and impairs spatial learning in transgenic mice. Learn Mem 2:26–39.

Gregory WA, Edmondson JC, Hatten ME, Mason CA. 1988. Electron microscopic analysis of video-observed identified neurons migrating along glia in vitro. J Neurosci 8:1728–1738.

Grosche J, Kettenmann H, Reichenbach A. 2002. Bergmann glia form distinct morphological structures to interact with cerebellar neurons. J Neurosci Res 68:138–149.

Grosche J, Matyash V, Moller T, Verkhratsky A, Reichenbach A, Kettenmann H. 1999. Microdomains for neuron-glia interaction: Parallel fiber signaling to Bergmann glial cells. Nat Neurosci 2:139–143.

Haber M, Zhou L, Murai KK. 2006. Cooperative astrocyte and dendritic spine dynamics at hippocampal excitatory synapses. J Neurosci 26:8881–8891.

Halassa MM, Fellin T, Takano H, Dong JH, Haydon PG. 2007. Synaptic islands defined by the territory of a single astrocyte. J Neurosci 27:6473–6477.

Harrington AW, Kim JY, Yoon SO. 2002. Activation of Rac GTPase by p75 is necessary for c-jun N-terminal kinase-mediated apoptosis. J Neurosci 22:156–166.

Hatten ME, Mason CA. 1990. Mechanisms of glial-guided neuronal migration in vitro and in vivo. Experientia 46:907–916.

He TC, Zhou S, da Costa LT, Yu J, Kinzler KW, Vogelstein B. 1998. A simplified system for generating recombinant adenoviruses. Proc Natl Acad Sci USA 95:2509–2514.

Hirrlinger J, Hulsmann S, Kirchhoff F. 2004. Astroglial processes show spontaneous motility at active synaptic terminals in situ. Eur J Neurosci 20:2235–2239.

Iino M, Goto M, Kakegawa, Okado H, Sudo M, Ishiuchi S, Miwa A, Takayasu Y, Saito I, Tsuzuki K, Ozowa S. 2001. Glia-synapse interaction through Ca^{2+}-permeable AMPA receptors in Bergmann glia. Science 292:926–929.

Laming PR, Kimelberg H, Robinson S, Salm A, Hawrylak N, Muller C, Roots B, Ng K. 2000. Neuronal-glial interactions and behaviour. Neurosci Biobehav Rev 24:295–340.

Lin SC, Bergles DE. 2004. Synaptic signaling between GABAergic interneurons and oligodendrocyte precursor cells in the hippocampus. Nat Neurosci 7:24–32.

Lordkipanidze T, Dunaevsky A. 2005. Purkinje cell dendrites grow in alignment with Bergmann glia. Glia 51:229–234.

McCall MA, Gregg RG, Behringer RR, Brenner M, Delaney CL, Galbreath EJ, Zhang CL, Pearce RA, Chiu SY, Messing A. 1996. Targeted deletion in astrocyte intermediate filament (Gfap) alters neuronal physiology. Proc Natl Acad Sci USA 93:6361–6366.

Murai KK, Nguyen LN, Irie F, Yamaguchi Y, Pasquale EB. 2003. Control of hippocampal dendritic spine morphology through ephrin-A3/EphA4 signaling. Nat Neurosci 6:153–160.

Nestor MW, Mok LP, Tulapurkar ME, Thompson SM. 2007. Plasticity of neuron-glial interactions mediated by astrocytic EphARs. J Neurosci 27:12817–12828.

Nishida H, Okabe S. 2007. Direct astrocytic contacts regulate local maturation of dendritic spines. J Neurosci 27:331–340.

O'Kane EM, Stone TW, Morris BJ. 2003. Distribution of Rho family GTPases in the adult rat hippocampus and cerebellum. Brain Res Mol Brain Res 114:1–8.

Peters A, Palay SL, Webster HD. 1976. The fine structure of the nervous system: The neurons and supporting cells. Philadelphia: W. B. Saunders. p 406.

Pfrieger FW, Barres BA. 1997. Synaptic efficacy enhanced by glial cells in vitro. Science 277:1684–1687.

Piet R, Jahr CE. 2007. Glutamatergic and purinergic receptor-mediated calcium transients in Bergmann glial cells. J Neurosci 27:4027–4035.

Rakic P. 1971. Neuron-glia relationship during granule cell migration in developing cerebellar cortex. A golgi and electronmicroscopic study in Macacus rhesus. J Comp Neurol 141:283–312.

Shibuki K, Gomi H, Chen L, Bao S, Kim JJ, Wakatsuki H, Fujisaki T, Fujimoto K, Katoh A, Ikeda T, Chen C, Thompson RF, Itohara S. 1996. Deficient cerebellar long-term depression, impaired eyeblink conditioning, and normal motor coordination in GFAP mutant mice. Neuron 16:587–599.

Spacek J. 1985. Three-dimensional analysis of dendritic spines. III. Glial sheath. Anat Embryol (Berl) 171:245–252.

Takatsuru Y, Takayasu Y, Iino M, Nikkuni O, Ueda Y, Tanaka K, Ozawa S. 2006. Roles of glial glutamate transporters in shaping EPSCs at the climbing fiber-Purkinje cell synapses. Neurosci Res 54:140–148.

Takayasu Y, Iino M, Shimamoto K, Tanaka K, Ozawa S. 2006. Glial glutamate transporters maintain one-to-one relationship at the climbing fiber-Purkinje cell synapse by preventing glutamate spillover. J Neurosci 26:6563–6572.

Tashiro A, Yuste R. 2004. Regulation of dendritic spine motility and stability by Rac1 and Rho kinase: Evidence for two forms of spine motility. Mol Cell Neurosci 26:429–440.

Thompson SM. 2003. Ephrins keep dendritic spines in shape. Nat Neurosci 6:103–104.

Ullian EM, Sapperstein SK, Christopherson KS, Barres BA. 2001. Control of synapse number by glia. Science 291:657–661.

Ventura R, Harris KM. 1999. Three-dimensional relationships between hippocampal synapses and astrocytes. J Neurosci 19:6897–6906.

Yamada K, Fukaya M, Shibata T, Kurihara H, Tanaka K, Inoue Y, Watanabe M. 2000. Dynamic transformation of Bergmann glial fibers proceeds in correlation with dendritic outgrowth and synapse formation of cerebellar Purkinje cells. J Comp Neurol 418:106–120.

Yang Y, Ge W, Chen Y, Zhang Z, Shen W, Wu C, Poo M, Duan S. 2003. Contribution of astrocytes to hippocampal long-term potentiation through release of D-serine. Proc Natl Acad Sci USA 100:15194–15199.

Zhang JM, Wang HK, Ye CQ, Ge W, Chen Y, Jiang ZL, Wu CP, Poo MM, Duan S. 2003. ATP released by astrocytes mediates glutamatergic activity-dependent heterosynaptic suppression. Neuron 40:971–982.